Astronomy & Astrophysics manuscript no. ms June 9, 2009
(DOI: will be inserted by hand later)

The Radial Distribution of the Two Stellar Populations in NGC 1851 ⋆

A. P. Milone[1], P. B. Stetson[2], G. Piotto[1], L. R. Bedin[3], J. Anderson[3], S. Cassisi[4], and M. Salaris[5]

[1] Dipartimento di Astronomia, Università di Padova, Vicolo dell'Osservatorio 3, Padova, I-35122, Italy
[2] Dominion Astrophysical Observatory, Herzberg Institute of Astrophysics, National Research Council, 5071 West Saanich Road, Victoria, BC V9E 2E7, Canada
[3] Space Telescope Science Institute, 3700 San Martin Drive, Baltimore, MD 21218, USA
[4] INAF-Osservatorio Astronomico di Collurania, Via M. Maggini, Teramo I-64100, Italy
[5] Astrophysics Research Institute, Liverpool John Moores University, Twelve Quays House, Egerton Wharf, Birkenhead CH41 1LD, UK

Received Xxxxx xx, xxxx; accepted Xxxx xx, xxxx

Abstract. We have analyzed ACS/WFC and WFPC2 images from *HST*, as well as ground-based data to study the radial distribution of the double sub-giant branch (SGB) recently discovered in the Galactic globular cluster NGC 1851. We found that the SGB split can be followed all the way from the cluster center out to at least 8′ from the center. Beyond this distance out to the tidal radius at ∼ 11.7 arcmin, there are simply too few SGB stars to identify the sequences. The number ratio of the bright SGB to the faint SGB stars shows no significant radial trend. Furthermore, we have found that the ratio of blue horizontal-branch (HB) stars plus RR Lyrae to the red HB stars also remains constant from the cluster center to the outer envelope.

1. Introduction

Precise Hubble Space Telescope (*HST*) photometry has provided evidence that NGC 1851 hosts two distinct subpopulations of stars (Milone et al. 2008) as indicated by a clear bifurcation of the sub-giant branch (SGB) in its color magnitude diagram (CMD). This discovery has sparked new interest in this object and, consequently, numerous efforts aimed at better understanding how this cluster formed and evolved.

Milone et al. (2008) suggest that two star-formation episodes delayed by about one Gyr could explain the observed split of the SGB. As an alternative scenario, Cassisi et al. (2008) suggest that the SGB split can be explained by the presence of two stellar populations, one with normal α-element enhancement, and the other characterized by a peculiar CNONa chemical pattern with C+N+O abundance increased by a factor of ∼ 2. Two such populations could account for the observed bright and faint SGB (hereafter bSGB and fSGB), respectively, without requiring any significant age difference.

Interestingly, this latter scenario seems to be supported by early spectroscopic measurements (Hesser et al. 1982) which indicate the presence of two groups: CN-strong and CN-weak stars. In addition, the work of Calamida et al. (2007) shows that in the Strömgren (m_1, $u - y$) CMD, the red giant branch (RGB) of NGC 1851 splits into two sequences that, like the SGB split, can be explained by two populations with different CN abundances.

A more recent spectroscopic investigation by Yong & Grundahl (2008) determined the chemical composition for eight bright giants in NGC 1851. Their analysis revealed large star-to-star light-element-abundance differences of the elements Zr and La. These *s*-process elements are correlated with Al and anticorrelated with O. Furthermore, the Zr and La abundances appear to peak around two distinct values. Yong et al. (2009) show that the C+N+O abundance exhibits a large spread (∼ 0.6 dex), giving further support to the Cassisi et al. (2008) scenario. They also found a correlation of Na, Al, Zr, La abundance with C+N+O, as expected in the scenario in which intermediate mass AGB stars are responsible for globular-cluster light-element abundance variation.

Another important peculiarity of NGC 1851 is that it is one of only a few examples of a bimodal horizontal branch (HB) cluster. On the basis of detailed numerical simulations, Salaris et al. (2008) found that it is possible to account simultaneously for the various empirical constraints such as the HB morphology, the star counts along the HB as well as the ratio between faint SGB stars and bright SGB ones,if all the upper SGB stars and a small fraction of lower SGB stars evolves into the red HB, while most of the lower SGB stars populates the blue HB (including the RR Lyrae variables).

Therefore it is tempting to associate the bSGB stars with the CN-normal, *s*-process-normal stars and with the red HB, while

Send offprint requests to: A. P. Milone

⋆ Based on observations with the NASA/ESA *Hubble Space Telescope*, obtained at the Space Telescope Science Institute, which is operated by AURA, Inc., under NASA contract NAS 5-26555, under GO-11233.

the fainter SGB should be populated by CN-strong, *s*-process-element-enhanced stars which should evolve mainly onto the blue HB. This scenario implies that fSGB stars correspond to the second generation and that they formed from material processed through a first generation of stars.

The study of the spatial distribution of the two stellar populations associated with the double SGB occupies a pivotal role in the current research on multiple stellar populations in GCs. Milone et al. (2008) studied a CMD containing stars with radial distances smaller than ∼2.5 arcmin from the cluster center. In this paper, we extend the analysis to the outermost regions of the cluster. Our radial extension covers the whole cluster from the center to beyond the tidal radius (r_{tidal}=11.7 arcmin, Harris 1996, 2003).

A first attempt at constraining the radial distribution of the two stellar populations associated with the double SGB comes from the recent work by Zoccali et al. (2009). They analyzed VLT-FORS *V*, *I* images, of the South West quadrant of the cluster with the aim of following the extent of the double SGB from ∼1 to ∼13 arcmin from the cluster center. Zoccali et al. (2009) claimed that the percentage of fSGB stars, which is ∼45% in the innermost region decreases at ∼1.5 arcmin from the center and completely disappears at ∼ 2.4 arcmin. The more extensive and higher-precision data set presented below does not confirm the results of Zoccali et al. (2009).

The plan of the paper is as follows. In the next section we describe the data and the data reduction. The CMDs from different data sets are presented in Sect. 3. In Sect. 4 we describe the criteria used to define the NGC 1851 sub-populations and how we measured their relative frequency at several radial distances. We present the radial distribution of the two stellar populations in NGC 1851 and discuss our results in Sect. 5.

Table 1. Description of the *HST* data sets used in this paper.

INSTR	DATE	N×EXPTIME	FILT	PROGRAM (PI)
ACS/WFC	May 01 2006	20s+5×350s	F606W	10775 (Sarajedini)
ACS/WFC	May 01 2006	20s+5×350s	F814W	10775 (Sarajedini)
WFPC2	Nov 07 2007	10×230s	F450W	11233 (Piotto)
WFPC2	Nov 07 2007	5×200s+5×230s	F814W	11233 (Piotto)

2. Observation and data reduction

In order to study the radial distribution of SGB and HB stars in NGC 1851, we considered three distinct data sets.

To probe the most crowded regions of the cluster we took advantage of the high resolving power of *HST*, using images collected with the Wide Field Channel (WFC) of the Advanced Camera for Survey (ACS) and with the Wide Field Planetary Camera 2 (WFPC2). NGC 1851 is not in a particularly dense region of the Galaxy ($l^{\rm II} = 245°, b^{\rm II} = -35°$), and ground-based observations can provide photometry outside the crowded central region with precision comparable to that of the more central regions observed with the *HST* cameras.

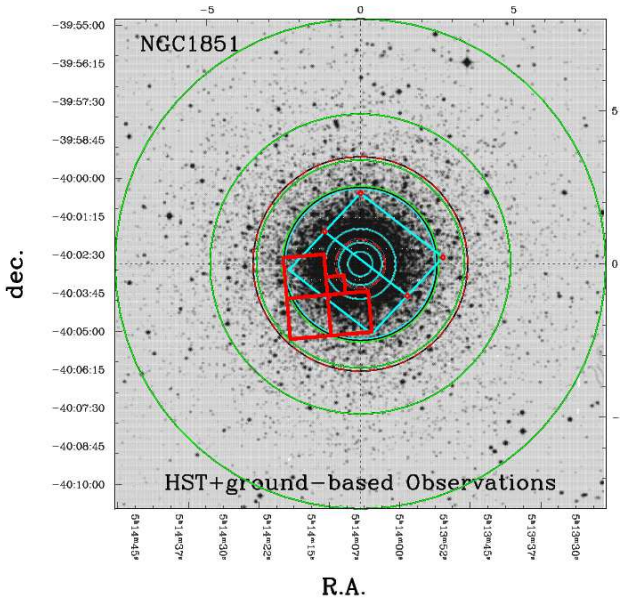

Fig. 1. For the innermost 8 arcmin, we show the footprints of the *HST*-images used in this paper superposed on a DSS image. In cyan ACS/WFC (circles highlight the corners of the first chip of ACS), in red WFPC2. Large circles show the different radial bins described in Section 4. The different colors refer to different data-sets: cyan for ACS/WFC, red for WFPC2, and green for ground-based data-set.

A brief description of the *HST* images used in this work is given in Table 1, while Fig. 1 shows a finding-chart of their footprints.

2.1. The ACS/WFC data-set

The *HST* ACS/WFC images come from GO-10775 (PI: Sarajedini, see also Sarajedini et al. 2007) and were presented in Milone et al. (2008); we have used the output of the reduction described in Anderson et al. (2008). In brief, the procedure analyzes all the exposures of each cluster simultaneously to generate a single list of stars for each field. Stars are measured independently in each image by using the best available PSF models from Anderson & King (2006).

This routine was designed to work well in both crowded and uncrowded fields, and it is able to detect almost every star that can be perceived by eye. It takes advantage of the many independent dithered pointings of each scene and the knowledge of the PSF to avoid including artifacts in the list. Calibration of ACS photometry into the Vega-mag system was performed following recipes in Bedin et al. (2005) and using the zero points given in Sirianni et al. (2005).

2.2. The WFPC2 data-set

The *HST* WFPC2 images come from GO-11233 (PI: Piotto), a proposal specifically dedicated to photometric detection of multiple populations.

The WFPC2 images have been reduced following the method of Anderson & King (2000), which is based on effective-point-spread-function fitting. We corrected for the 34^{th} row error in WFPC2 CCDs (see Anderson & King 1999 for details) and used the best distortion solution available, as given by Anderson & King (2003). Photometric calibration has been done according to the Holtzman et al. (1995) Vega-mag flight system for WFPC2 camera.

2.3. The ground-based data-set

The ground-based data are taken from the image archive maintained by one of us (Stetson 2000). The observations used here include 545 images from 14 observing runs with the Max Planck 2.2m telescope, the CTIO 4m, 1.5m, and 0.9m telescopes, and the Dutch 0.9m telescope on La Silla. Any given star may have as many as 69 independent measurements in the B filter, 78 in V, and 56 in I; among these, 62, 70, and 56, respectively, were taken on occasions that were judged to be of photometric quality. These data were reduced following the protocol outlined in some detail in Stetson (2005). We have complete photometric coverage of the cluster field out to a radius of 14.5 arcmin, and partial coverage to 25.9 arcmin, but we will restrict our discussion here to the area within 12.5 arcmin, which is slightly larger than the tidal radius of 11.7 arcmin.

3. The CMDs

Figure 2 shows the CMDs from *HST* observations that cover the densest regions of the cluster. The left panel shows the CMD already published by Milone et al. (2008), and the right panel shows the newly derived CMD from the WFPC2 data described in Sect. 2.2.

The CMDs from ground-based photometry are shown in Fig. 3, where we have rejected all the stars within 2.5 arcmin from the cluster center. The split of the SGB is clearly visible both in the $(V-I)$ vs. V and the $(B-I)$ vs. V CMD, and the split region is highlighted in the inset where we show a zoom of the SGB region. Note that the fact that we see the SGB split beyond $\sim$ 2.5 arcminutes is already in disagreement with the claims by Zoccali et al. (2009) who analysed the S-W quadrant and found no evidence for the presence of fSGB stars at radial distances larger than $\sim$ 2.4 arcmin. The left panel of Fig. 4 shows our V vs $(B-I)$ CMD from ground based data for stars with radial distance from the cluster center larger than 2.5 arcmin. We marked in red the stars that more likely belong to the fSGB. In the four right panels we plot the same CMD for stars in the four quadrants. The quoted numbers are the number of selected fSGB stars with Poisson errors. Because of the uncertainties we conclude that there is not significant difference in the distribution in the CMD of fSGB stars in the four quadrants. We detected 23 probable fSGB stars in the S-W field covered by Zoccali et al. (2009) most of them belonging to the lower part of the fSGB. Possibly, the difference between our result and the one obtained by Zoccali et al (2009) comes from the small number of fSGB stars with radial distance greater than $\sim$2.5 arcmin in the SW quadrant. It must be noted that the CMD of Zoccali et al. (2009) have likely larger photometric errors than in our case, because their photometry comes from a short (2s) and a long (15s) FORS2-VLT image in V and I bands. Their larger photometric errors make difficult the identification of fSGB stars especially in the lower part of the SGB where the faint and the bright SGB have a smaller color difference.

The CMD in the right panel of Fig. 3 suggests that the RGB of NGC 1851 has some spread in the $B-I$ color. This spread could be related to the presence of the two RGB branches observed by Calamida et al. (2007) in the Strömgren (m_1, $u-y$) CMD which is possibly associated with the presence of two groups of stars with different CN abundances (Yong & Grundahl 2008). To investigate how the upper and lower SGB populations may vary with radius, we divided the cluster into seven concentric annuli. The inner three are covered by the ACS data set out to 2.5 arcmin, and the outer four are covered by the ground-based data set, going out to 12.5 arcmin. In Fig. 5 we show the CMD of the region around the SGB for stars in each annulus. Both the fainter and the brighter SGBs are clearly visible for radial distances smaller than $\sim$8 arcmin. Beyond this radius, the number of stars is simply too small to distinguish any feature of the SGB. The WFPC2 observations allow an additional check on the distribution of stars along the SGB in the interval between 0.8 and 3.5 arcmin (see the central panel in Fig. 5).

4. Radial distribution of the population ratio

4.1. The SGB subpopulations

To determine the fraction of fSGB and bSGB stars, we adopted a procedure similar to that used by Milone at al. (2009). Fig. 6 illustrates this four-step procedure for the ACS/WFC sample.

We selected by hand two points on the fSGB ($P_{1,f}$,$P_{2,f}$) and two points on the bSGB ($P_{1,b}$,$P_{2,b}$) with the aim of delimiting the SGB region where the split is most evident. These points define the two lines in panel (a), and only stars contained in the region between these lines were used in the following analysis.

In panel (b) we have transformed the CMD linearly (the transformation equation is given in Appendix) into a reference frame where: the origin corresponds to $P_{1,b}$; $P_{1,f}$ is mapped into (1,0), and the coordinates of $P_{2,b}$ and $P_{2,f}$ are (0,1) and (1,1) respectively. For convenience, in the following, we indicate as 'abscissa' and 'ordinate' the abscissa and the ordinate of this reference frame. The dashed green line is the fiducial of the bSGB. We drew it by marking several points on the bSGB, and interpolating a line through them by means of a spline fit. The black lines of panel (a) correspond to the loci with 'abscissa' of zero and one and to the loci with 'ordinate' of zero and one.

In panel (c) we have calculated the difference between the 'abscissa' of each star and the 'abscissa' of the fiducial line (Δ 'abscissa').

The histograms in panel (d) are the distributions in Δ 'abscissa' for stars in four Δ 'ordinate' intervals. These distributions have been modeled as the sum of two partially overlapping Gaussian functions. To reduce the influence of outliers (such as stars with poor photometry, field stars and binaries) we did a preliminary fit of the Gaussian distribution using all available stars. Then we rejected all the stars more than two σ_b

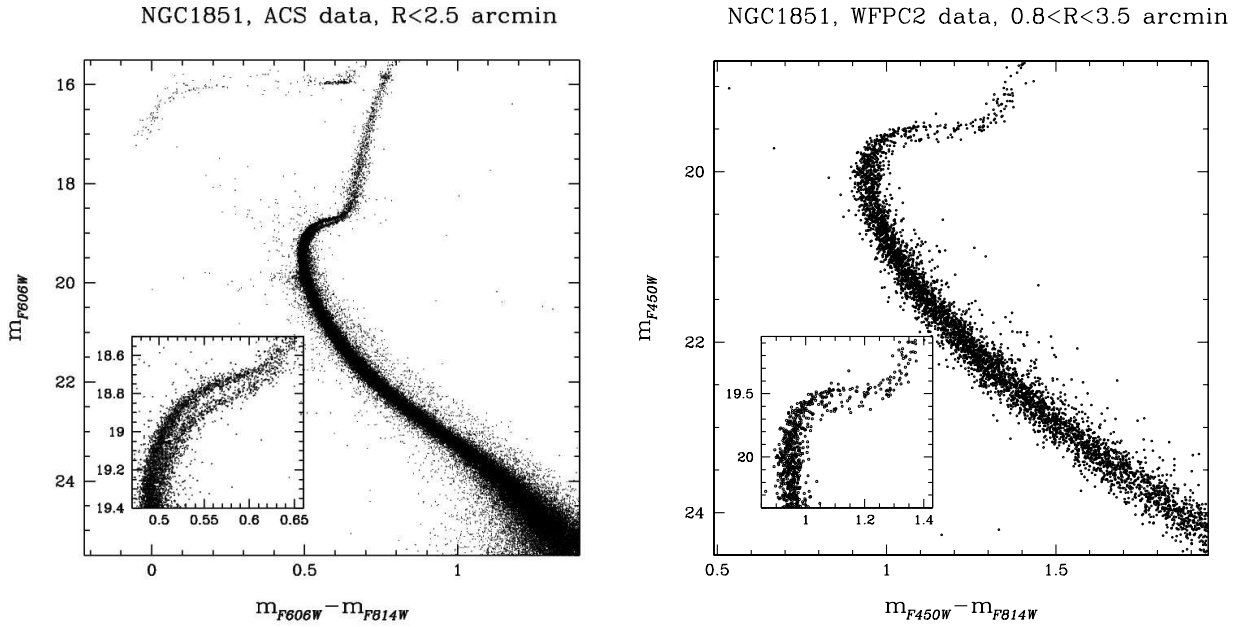

Fig. 2. CMD of NGC 1851 from ACS (*left*) and WFPC2 (*right*) data. The inset show a zoom around the SGB region.

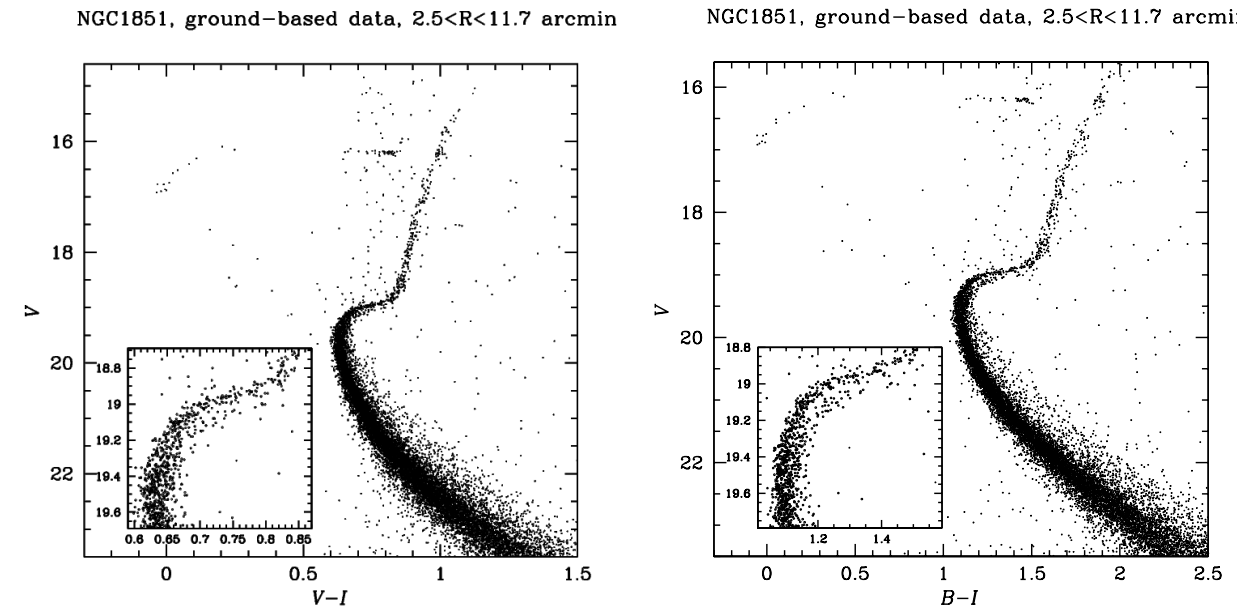

Fig. 3. *V* vs. $V-I$ (*left*) and *V* vs. $B-I$ (*right*) CMD of NGC 1851 from ground-based data. The inset show a zoom around the SGB region. Only stars with radial distance greater than 2.5 arcmin are plotted.

to the left of the bSGB and more than two σ_f to the right of the fSGB and repeated the fit (the σ's are those of the best fitting Gaussian in each Δ'ordinate' bin fitted to the fSGB and bSGB respectively). In panel (c) the continuous vertical lines indicate the centers of the best-fitting Gaussians in each Δ'ordinate' interval. The red dashed line is located two σ_b on the left side of the bSGB, and the blue dashed line runs two σ_f on the right side of the fSGB.

We repeated the procedure for the ground-based sample, as illustrated in Figure 7. In this case we have reduced the number of bins in 'magnitude' to just two intervals, because of the smaller number of stars. The same procedure has also been applied to the WFPC2 data. In this case, we use the entire data set, without splitting it into bins, as illustrated in Fig. 8.

It is important to notice that each of the points $P_{1,b}$, $P_{1,f}$, $P_{2,b}$, and $P_{2,f}$—which we have arbitrarily defined with the sole purpose of isolating a group of stars representative of each of the two SGBs—corresponds to a different mass ($\mathcal{M}_{P1b}$, $\mathcal{M}_{P1f}$, $\mathcal{M}_{P2b}$, and $\mathcal{M}_{P2f}$).

To obtain a more accurate measure of the fraction of stars in each of the two populations (hereafter: $f_{\rm bSGB}$, $f_{\rm fSGB}$) we have to compensate for the fact that the two stellar groups that define the two SGBs cover two different mass intervals ($\mathcal{M}_{P2f}-\mathcal{M}_{P1f} \neq \mathcal{M}_{P2b}-\mathcal{M}_{P1b}$), due to the different evolution-

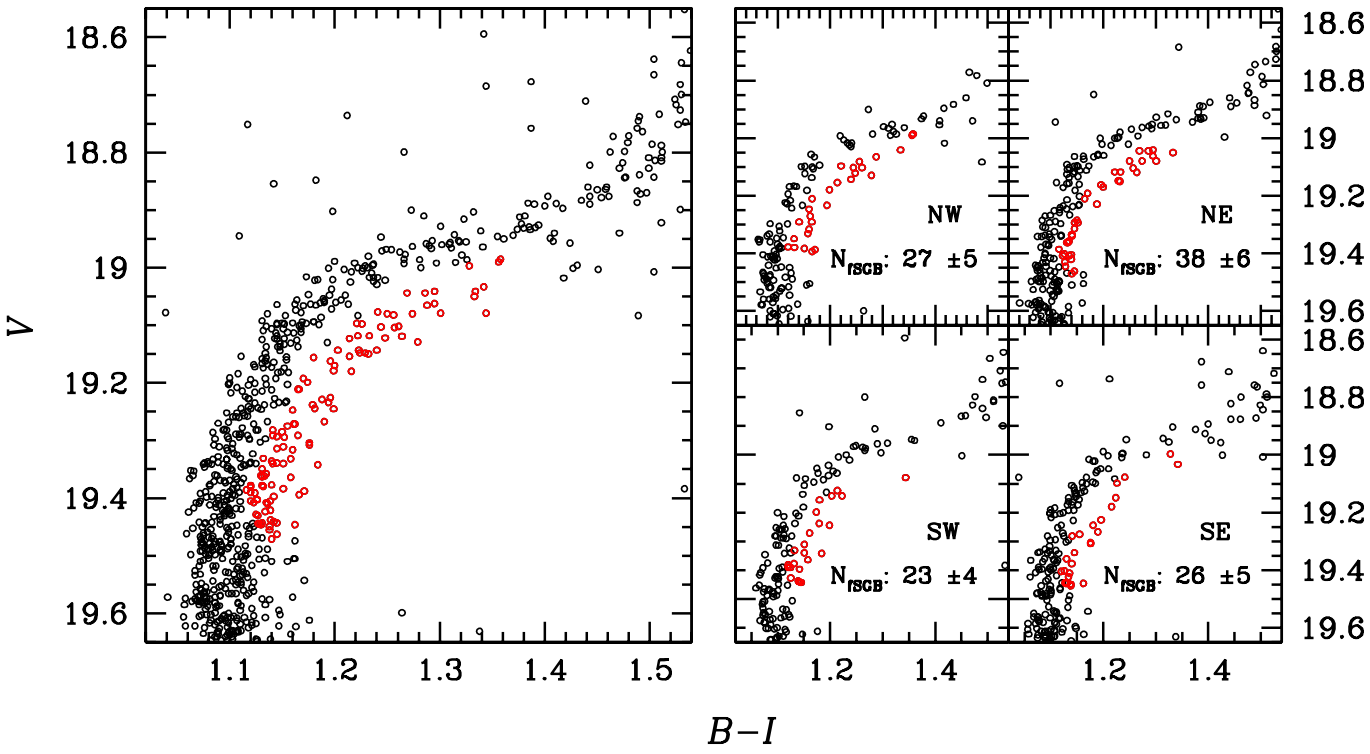

Fig. 4. V vs. $B-I$ CMD of NGC 1851 from ground-based data for stars with radial distances from the cluster center larger than 2.5 arcmin (*left*) and CMDs the four quadrants *right*.

ary lifetimes. Consequently, the correction we have to apply will be somewhat dependent on the choice of the mass function.

To this end, we can calculate the fraction of stars in each branch as:

$$f_{\rm bSGB} = \frac{\frac{A_b}{N_b/N_f}}{A_f+\frac{A_b}{N_b/N_f}}$$
$$f_{\rm fSGB} = \frac{A_f}{A_f+\frac{A_b}{N_b/N_f}}$$

where A_b and A_f are the areas of the Gaussians that best fit the bSGB and the fSGB, and $N_{f(b)} = \int_{P_{1,f(b)}}^{P_{2,F(b)}} \phi(\mathcal{M})d\mathcal{M}$.

As for the dependence on the adopted mass function, we ran the following test. Because of the effect of mass segregation, we assumed a heavy-mass-dominated mass function for the central regions ($\alpha = -1.0$), and a steep ($\alpha = 3.35$) mass function for the external regions. Even with these extreme assumptions, we found that the mass function effect can change the relative fSGB/bSGB population ratio by a negligible 4%, in the small mass interval covered by our SGB stellar groups. Therefore, for simplicity, we adopted a Salpeter (1955) IMF for $\phi(\mathcal{M})$.

Since the inferred population ratio depends on the assumed evolutionary lifetimes, our result is necessarily somewhat model-dependent. In fact, the values could even be scenario dependent as well. Cassisi et al. (2008) propose that the two SGBs in NGC 1851 could in principle be explained by one of the following scenarios:

- A) the bSGB and the fSGB are both populated by two normal α-enhanced stellar populations with ages of 10 and 11 Gyrs, respectively;
- B) the fSGB belongs to an 11 Gyr old, normal α-enhanced stellar population, while the bSGB belongs to a population 2 Gyr younger with high C+N+O abundances;
- C) the bSGB and the fSGB both correspond to a 10 Gyr old, normal α-enhanced stellar population, but the fSGB population has C+N+O abundances a factor of two higher than the bSGB population.

Salaris et al. (2008) found that scenario C does the best job of reproducing both the spectroscopic and photometric observations, while scenario B seems the least consistent with the data. Regardless, these three possibilities illustrate that inferring the *actual* frequency ratio of the populations depends upon the assumed astrophysical explanation of the difference between them, through the different implications for the evolutionary lifetimes between our empirically chosen fiducial evolutionary states.

To better characterize the radial distribution of SGB stars we divided both the ACS and ground-based data into concentric annuli as indicated in Fig. 1. The radial intervals have been chosen so that the each of the four ACS bins have the same number of stars, and the three ground-based bins also have the same number of stars among themselves. In each of these annuli, we calculated the fraction of bSGB and fSGB stars using the procedure described above. Table 2 summarizes the results. The first two columns list the radial interval and the average radial distance for SGB stars within this radial interval (R_{AVE}). The origin of the data and the number of SGB stars in each bin

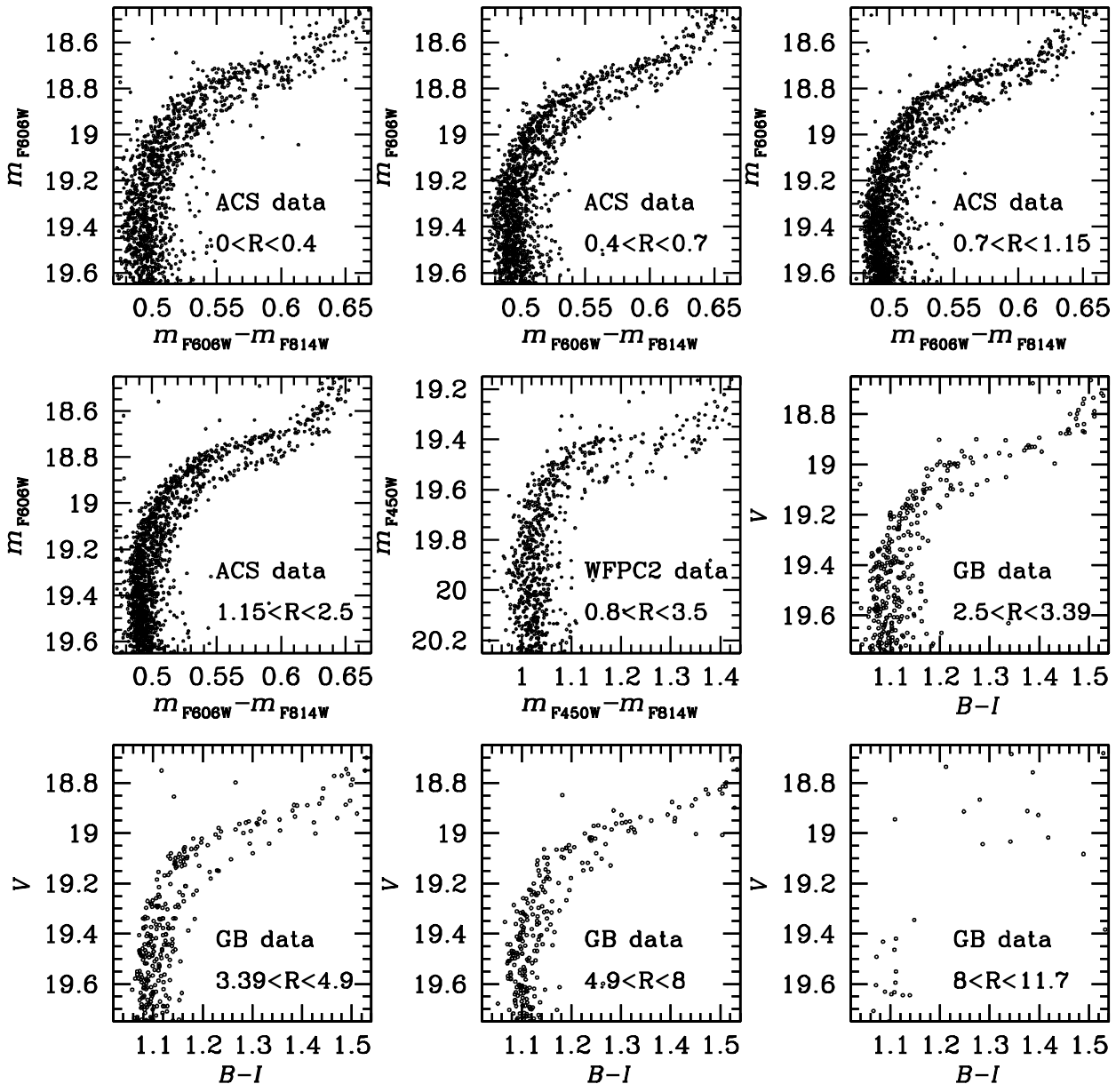

Fig. 5. CMDs of the region around the SGB of NGC 1851 at different radial distances, from the center out to the tidal radius, and from the different data bases. The double SGB is visible out to where there are enough stars to see the SGB.

are indicated in the third and forth columns, respectively, while the last three columns list the ratio of faint to bright SGB stars that we obtain for each of the three scenarios of Cassisi et al. (2008).

Since the values of the subpopulation ratios depend on the mass interval corresponding to each SGB segment, the results differ slightly depending on whether we assume that the SGB split corresponds to scenario A, B, or C, as we use stellar masses from three different sets of isochrones. The main result of the paper is summarized in Fig. 9. Although Scenarios A and B show a hint of a slight radial gradient, it is not statistically significant. Scenario C does not even show a hint of a gradient. Even when we maximize our statistics by putting the ACS data in one bin, the WFPC2 photometry in a second bin, and all the ground-based data in a third bin (see first three rows in Table 2), there is no significant variation in the fSGB:bSGB ratio with cluster radius.

When comparing the three different scenarios, we note that the radial trends are slightly different. This has no reason to be, since different evolutionary times should not change the relative trends of the ratios. The problem comes from the fact that we are using three different data-sets, and we can not avoid

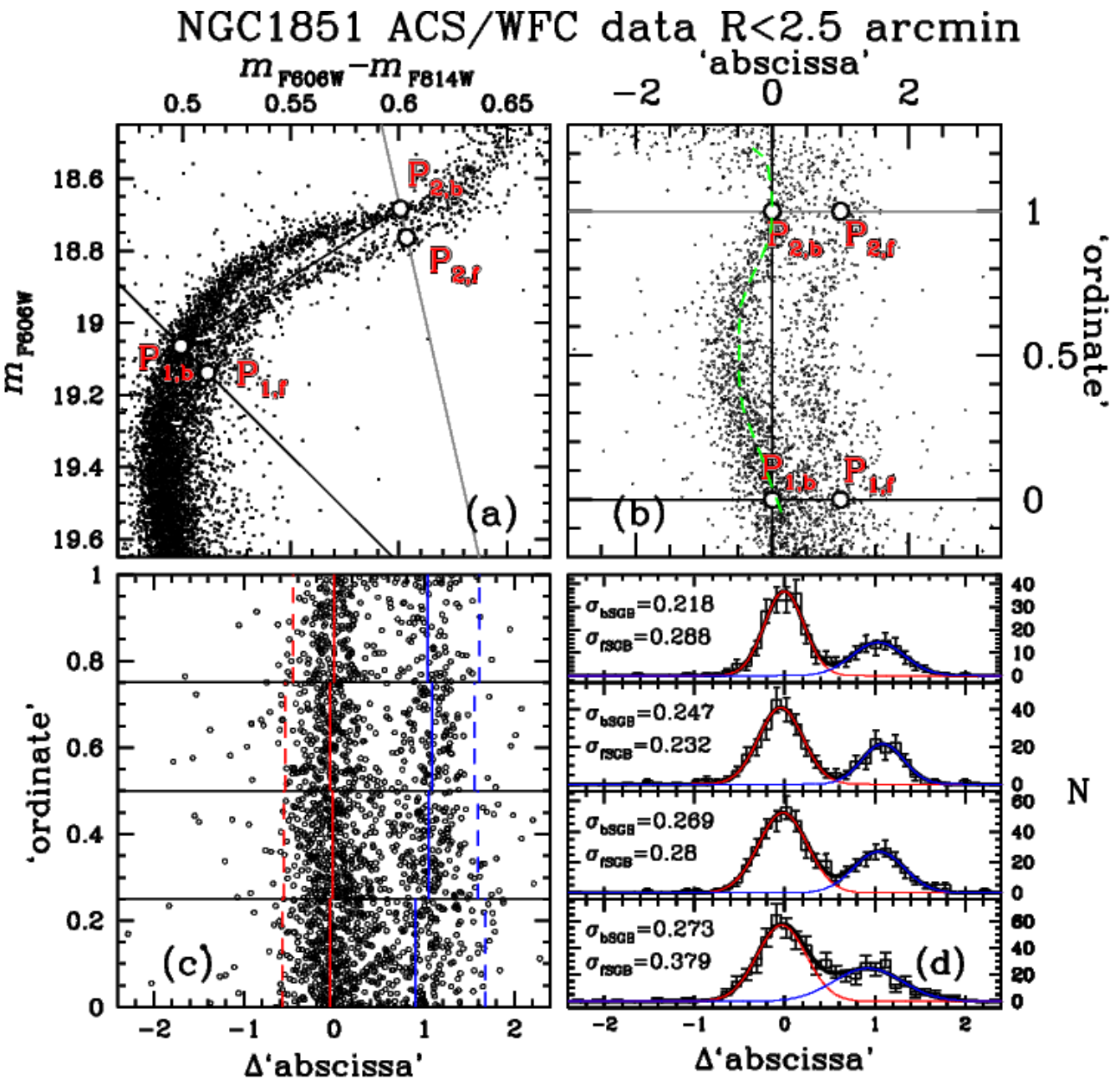

Fig. 6. This figure illustrates the procedure adopted to measure the fraction of stars belonging to the bSGB and fSGB in NGC 1851. Panel (a) shows a zoom of the ACS/WFC CMD. The two lines delimit the portion of the CMD where the split is most evident. Only stars from this region are used to measure the population ratio. In Panel (b) we have transformed the reference frame of Panel (a). The green dashed line is the fiducial of the region around the bSGB. In Panel (c) we plotted stars between the two lines but after the subtraction of the fiducial line 'abscissa' The four right bottom panels show the Δ'abscissa' distribution for stars in four Δ'ordinate' bins. The solid lines represent a bigaussian fit. For each bin, the dispersions of the best fitting Gaussian are indicated.

small transformation errors from theoretical to observational plane. ACS, WFPC2, and ground-based data require slightly different corrections because we are working with three different filter systems, and we have used the models to infer the relevant mass ranges. These uncertainties generate small systematic errors in our estimate of the fSGB:bSGB ratio. However, these errors are well within our estimated error bars, and do not change the main result of a flat trend.

We want to emphasize that the fractions of faint to bright SGB stars calculated in this paper and listed in Table 2 accurately account for the mass interval covered by each SGB segment. Therefore they differ from the numbers quoted in Milone

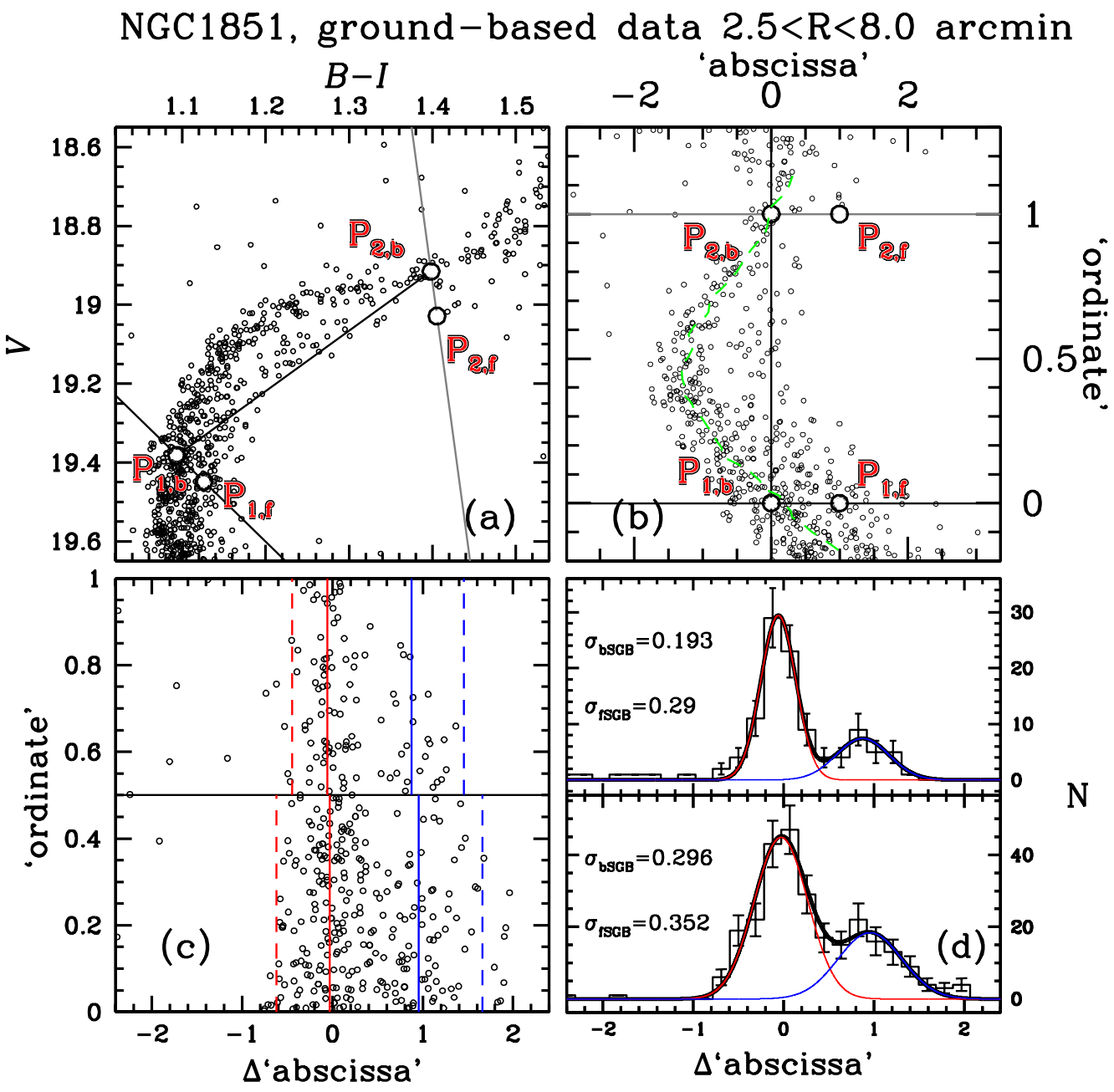

Fig. 7. As in Fig. 6 for stars from the ground-based sample and with 2.5<R<8.0 arcmin.

Table 2. Percentage of fSGB and bSGB stars at several radial distances.

R_{MIN} - R_{MAX}	R_{AVE}	$INSTR$	N_{SGB}	N_{fSGB}/N_{bSGB} (A)	N_{fSGB}/N_{bSGB} (B)	N_{fSGB}/N_{bSGB} (C)
0.0-2.5	0.80	ACS	1746	0.60±0.03	0.69±0.03	0.53±0.03
0.8-3.5	1.80	WFPC2	105	0.56±0.09	0.52±0.09	0.54±0.09
2.5-8.0		G-B	303	0.49±0.07	0.53±0.07	0.51±0.07
0.0-0.4	0.28	ACS	443	0.59±0.06	0.69±0.07	0.54±0.05
0.4-0.7	0.57	ACS	444	0.57±0.05	0.67±0.06	0.53±0.05
0.7-1.2	0.89	ACS	443	0.53±0.05	0.62±0.06	0.49±0.05
1.2-2.5	1.54	ACS	443	0.50±0.05	0.58±0.06	0.46±0.05
0.8 3.5	1.80	WFPC2	105	0.56±0.09	0.52±0.09	0.54±0.09
2.5 3.4	2.98	G-B	100	0.41±0.08	0.44±0.08	0.40±0.08
3.4 4.9	4.08	G-B	101	0.47±0.10	0.55±0.11	0.49±0.10
4.9 8.0	6.09	G-B	100	0.50±0.11	0.54±0.12	0.52±0.11

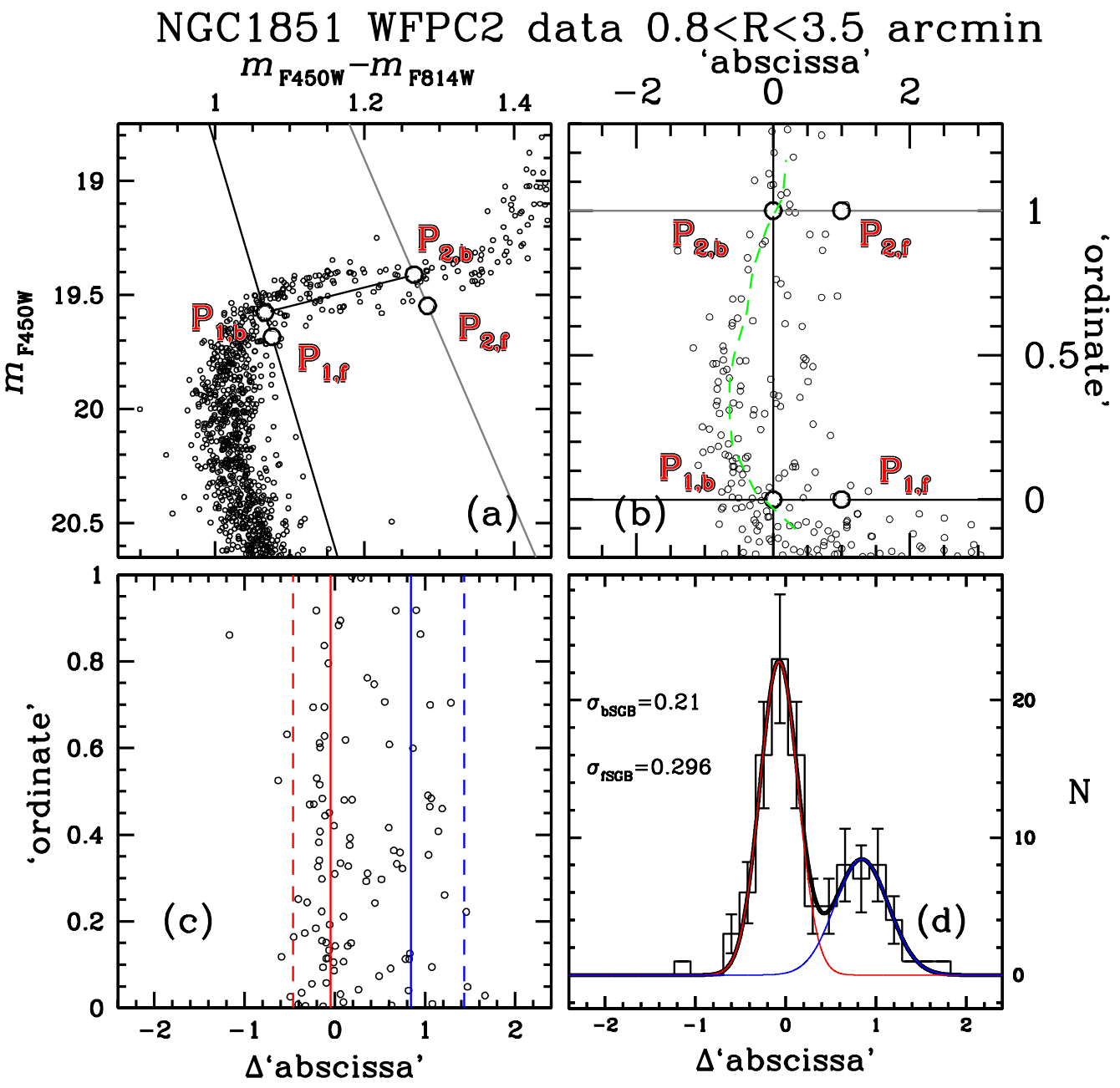

Fig. 8. As in Fig. 6 for stars with 0.8<R<3.5 arcmin. In this case we used the WFPC2 photometry.

et al. (2008) where we have simply determined the number of stars belonging to two segments of fSGB and bSGB in a given $m_{F606W} - m_{F814W}$ color interval.

4.2. The HB subpopulation

As we mentioned above, NGC 1851 is a prototypical bimodal HB cluster. In Fig. 10 we show the HB region for several annular bins both from ACS/WFC (top panels) and ground-based (bottom panels) data. Red HB stars are marked with red symbols, while blue HB stars and RR Lyrae are indicated in blue.

Table 3 lists the ratio between the blue HB stars plus RR Lyrae and red HB stars in three different radial annuli. In calculating these numbers we were careful to account for the fact that the lifetime of star in the blue HB is on average 11% greater than the lifetime in the red HB. This estimate has been obtained by comparing the core He-burning lifetime for the mean stellar mass populating the red HB with that of the mean stellar mass populating the blue HB in the HB synthetic models made by Salaris et al. (2008) for simulating the HB distribution in NGC1851.

The small number of intervals into which we have divided the field of view is a consequence of our need for a statisti-

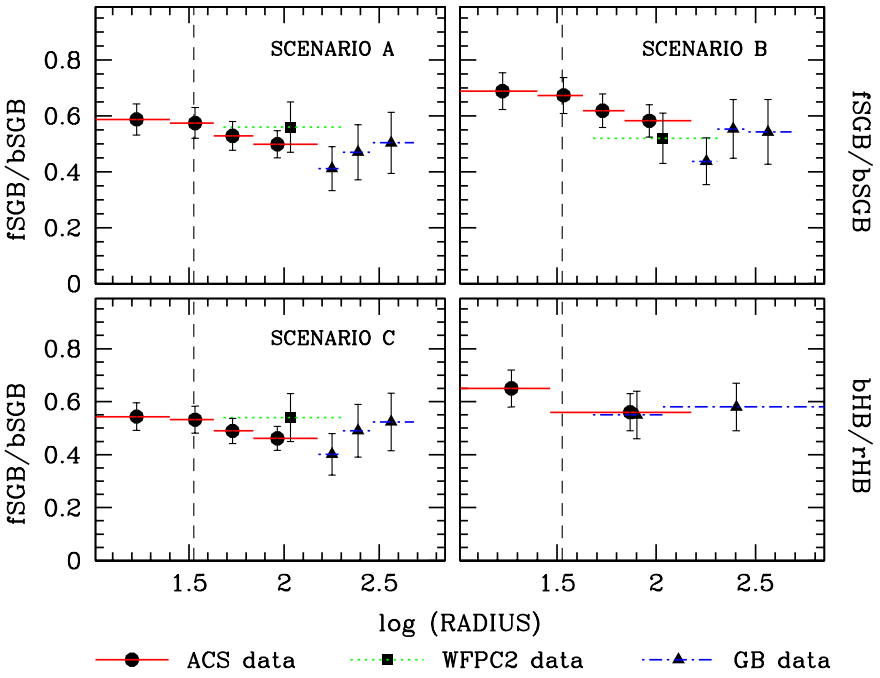

Fig. 9. Fraction of fainter over brighter SGB stars for the scenarios *A*, *B*, and *C* and fraction of blue HB over red HB. Circles, squares and triangles refer to the ACS/WFC, WFPC2 and WFI data sets. The dashed vertical lines mark the core and the half-mass radius.

cally significant number of stars in each subsample. The bottom right panel of Fig. 9 shows the trend of the (blue HB + RR Lyrae):(red HB) ratio as a function of the radial distance from the cluster center.

Note that for these bright objects we can now safely include the ground-based photometry within 2.5 arcmin from the cluster center, going as close as 0.8 arcmin, before crowding conditions become prohibitive even for these luminous stars. The overlap regions of the two data-sets, between 0.8 and 2.5 arcmin, provide us with an important cross-check on the solidity and consistency of the two independent sets of photometry.

Fig. 9 shows that there is no statistically significant evidence of a radial gradient in either the fSGB:bSGB ratio or the bHB:rHB ratio. Moreover, the results shown in Fig. 9 provide further support to the suggestion of Milone et al. (2008) and Salaris et al. (2008) that the blue HB stars are the progeny of the fSGB population, whilst the bulk of the red HB component is related to the bSGB population. More accurate spectroscopical measurements are mandatory in order to fully assess this scenario.

R_{MIN} - R_{MAX}	R_{AVE}	N	*INSTR*	$(HB_b + RRLy)/HB_r$
0.00 - 0.49	0.31	212	ACS	0.65±0.07
0.49 - 2.51	1.23	212	ACS	0.56±0.07
0.80 - 1.80	1.33	119	G-B	0.55±0.09
1.80 - 11.7	4.22	118	G-B	0.58±0.09

Table 3. Percentage of fSGB and bSGB stars at several radial distances.

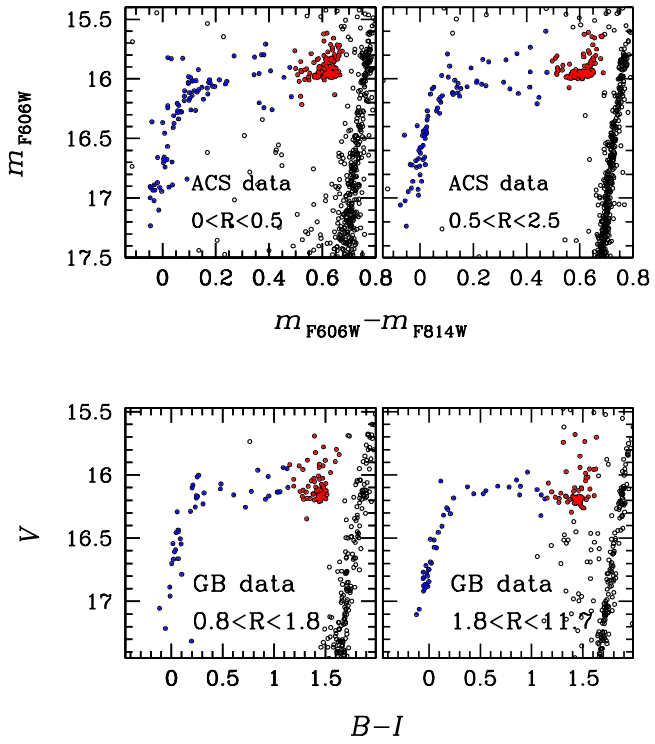

Fig. 10. Zoom of the CMD region around the HB at several radial distances from ACS (top) and WFI data (bottom). We indicated in red the probable red HB stars and RR Lyrae and in blue the probable blue HB stars.

5. Discussion

D'Ercole et al. (2008) have shown that if a second generation of stars is formed by material coming from or polluted by a first generation, then we would expect these stars to be born in the core of a stellar cluster, where a cooling flow collects the gas ejected by the earlier population. As the cluster evolves dynamically, the two populations mix and the ratio of second over first generation tends to a constant value in the inner part of the cluster. Until mixing is complete, the radial profile of this ratio is flat in the inner part and decreases in the outer cluster regions. By studying the radial profiles of the different populations, we might hope to see evidence of these initial gradients before dynamical relaxation washes them out.

Before this paper and the work by Zoccali et al. (2009), ω Centauri was the only cluster where the radial distribution of different stellar sub-populations had been analyzed. In ω Centauri the stellar population associated with the blue, more metal rich MS is more centrally concentrated than the red, more metal poor one, with the relative ratio of blue over red MS star counts being quite constant within the cluster core beyond ~ 12 arcmin and increasing by a factor of two from 8 arcmin (Sollima et al. 2007) to about 5 arcmin from the center. Then the blue MS to red MS ratio remains constant in the cluster core (Bellini et al. 2009).

In this paper, we have investigated the radial distribution of the two stellar populations associated with the double SGB of NGC 1851. By coupling *HST* and ground-based data we followed the distribution of the two populations from the center out to the tidal radius, both on the SGB and the HB. Salaris et al. (2008) claimed that the ratio of the two SGBs is consistent with the idea that the the progeny of the fSGB si distributed from the blue to the red HB, including the whole instability strip, while the bright one should be confined to the red. According to the scenario of Salaris et al. (2008), the fraction of fSGB that evolves into the red HB corresponds only to the 5% of the total number of stars.

At variance with Zoccali et al. (2009), we have clearly detected both the brighter and the fainter SGB at all radial distances, out to ~8 arcmin. At larger radii, the number of SGB stars is simply too small to detect any substructure in the SGB. We have determined the ratio of fainter to brighter SGB stars and, unlike the case with ω Centauri, found that—within the error bars—the two stellar populations have the same radial distribution. This conclusion does not depend on which of the three scenarios proposed by Cassisi et al. (2008) we assume to explain the observed SGB dichotomy. The ratio of the blue HB stars to the red HB stars also shows no significant trend with cluster radius.

Whatever the origin and formation process of the two stellar generations in NGC 1851, now the two groups seem to be well mixed within the cluster. Because of the short relaxation time of NGC 1851 (log t_{rh} ~ 8.8) this result may be not totally unexpected, as the cluster stars must be at least partially mixed. Unlike NGC 1851, ω Centauri has a very long relaxation time (log t_{rh} ~ 10), and it must have retained some information on the radial distribution of the gas from which its multiple stellar generations formed. However, only a detailed dynamical model, following the suggestion of D'Ercole et al. (2008) and Decressin et al. (2007), will answer the question of whether the gradient seen in Omega Cen and the lack of a gradient seen in NGC 1851 imply different initial radial distributions for the various populations.

Acknowledgements. The authors wish to thank Francesca D'Antona for useful discussion. We also thanks the anonymous referee for her/his comments and suggestions which helped to strenghen the results presented in this paper. APM and GP acknowledge support by PRIN2007 and ASI under the program ASI-INAF I/016/07/0. J.A. acknowledges support from STScI Grants GO-10775 and GO-11233.

References

Anderson, J., & King, I. R. 1999, PASP, 111, 1095
Anderson, J., & King, I. R. 2000, PASP, 112, 1360
Anderson, J., & King, I. R. 2003, PASP, 115, 113
Anderson, J., & King, I. R. 2006, PSFs, Photometry, and Astronomy for the ACS/WFC (ACS Instrument Science Rep. 2006-01; Baltimore: STScI)
Anderson, J. et al. 2008, AJ, 135, 2055
Bedin, L. R., Cassisi, S., Castelli, F., Piotto, G., Anderson, J., Salaris, M., Momany, Y. & Pietrinferni, A., 2005, MNRAS, 357, 1048
Bellini, A. et al., 2009, in preparation
Calamida, A., et al. 2007, ApJ, 670, 400
Cassisi, S., Salaris, M., Pietrinferni, A., Piotto, G., Milone, A. P., Bedin, L. R., & Anderson, J. 2008, ApJ, 672, L115
D'Ercole, A., Vesperini, E., D'Antona, F., McMillan, S. L. W. & Recchi, S. 2008 MNRAS391, 825
Decressin, T., Meynet, G., Charbonnel, C., Prantzos, N. & Ekström, S., 2007, A&A, 464, 1029
Harris, W. E., 1996, AJ, 112, 1487
Hesser, J. E., Bell, R. A., Harris, G. L. H. & Cannon, R., D. 1982, AJ, 87, 1470
Holtzman, J. A. et al. 1995, PASP, 107, 1065
Milone, A. P. et al. 2008, ApJ, 673, 241
Milone, A. P., Bedin, L. R., Piotto, G. & Anderson, J., 2009, A&A, 497, 755
Salaris, M., Cassisi, S., & Pietrinferni, A., 2008, ApJ, 678, L25
Salpeter, E. 1955, ApJ, 121, 161
Sarajedini, A. et al. 2007, AJ, 133, 1658
Sirianni, M. et al. 2005, PASP, 117, 1049
Sollima, A., Ferraro, F. R., Bellazini, M., Origlia, L., Straniero, O., & Pancino, E. 2007, ApJ, 654, 915
Stetson, P. B. 2000, PASP, 112, 925
Stetson, P. B. 2005, PASP, 117, 563
Yong, D., & Grundahal, F. 2008, ApJ, 672, L39
Yong, D., Grundahal, F., D'Antona, F., Karacas, A. I., Lattanzio, J. C., & Norris, J., E., 2009 ApJ, 695, L62
Zoccali, M., Pancino, E., Catelan, M., Hempel, M., Rejkuba, M., & Carrera, R., 2009 ApJ, 697, L22

Appendix Upon request from the referee, we give here the transformation equations used to pass from panel (a) to panel (b) in Figs. 6, 7, and 8. For simplicity we indicate the color and the magnitude as C and M respectively, and the 'abscissa' and the 'ordinate' as abs and ord.

$$abs = (CR - c2)/c3 \quad (1)$$

$$ord = yr/c1 \quad (2)$$

where:

$$CR = (C - C_{P1,b})\,cos\theta + (M - M_{P1,b})\,sin\theta \quad (3)$$

$$MR = -(C - C_{P1,b})\,sin\theta + (M - M_{P1,b})\,cos\theta \quad (4)$$

$$\theta = atan\frac{MR_{P1,b} - MR_{P2,b}}{CR_{P1,b} - CR_{P2,b}} \quad (5)$$

$$c1 = \frac{MR_{P2,b} - MR_{P2,f}}{CR_{P2,b} - CR_{P2,f}}CR + \frac{CR_{P2,b}MR_{P2,f} - CR_{P2,f}MR_{P2,b}}{CR_{P2,b} - CR_{P2,f}} \quad (6)$$

$$c2 = \frac{CR_{P1,b} - CR_{P2,b}}{ord_{P1,b} - ord_{P2,b}}ord + \frac{ord_{P1,b}CR_{P2,b} - ord_{P2,b}CR_{P1,b}}{ord_{P1,b} - ord_{P2,b}} \quad (7)$$

$$c3 = \frac{CR_{P1,f} - CR_{P2,f} - c2_{P1,f} + c2_{P2,f}}{ord_{P1,f} - ord_{P2,f}}ord + \frac{ord_{P1,f}(CR_{P2,f} - c2_{P2,f}) - ord_{P2,f}(CR_{P1,f} - c2_{P1,f})}{ord_{P1,f} - ord_{P2,f}} \quad (8)$$